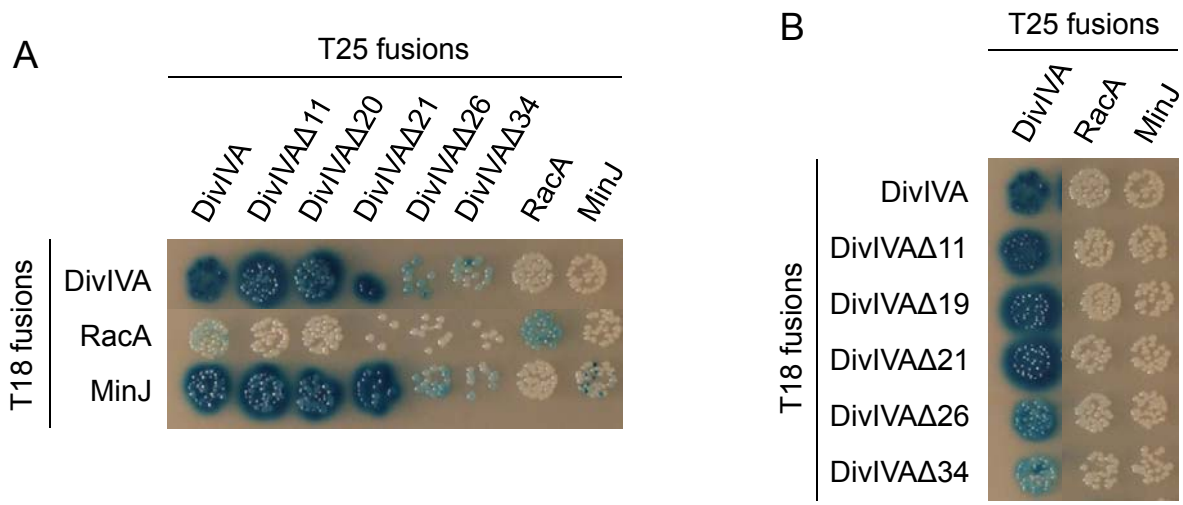

Fig. S1: Bacterial two hybrid analysis of the DivIVA interaction to MinJ and RacA. (A) The T25 plasmids p25-N-*divIVA* (full length DivIVA), pSBLH004 (DivIVAΔ11), pSBLH008 (DivIVAΔ20), pSBLH039 (DivIVAΔ21), pSBLH040 (DivIVAΔ26), and pSBLH041 (DivIVAΔ34), were co-transformed with the T18 plasmids pUT18C-*divIVA*, pUT18C-*racA*, and pUT18C-*minJ* in the *E. coli* strain BTH101 and aliquots of the transformation mixture were spotted onto nutrient agar plates containing ampicillin, kanamycin, IPTG and X-Gal (for details see materials and methods section). Images were taken after 40 h of incubation at 30°C. The T25 plasmids pKT25-*racA* and p25-N-*minJ* were used as self-interaction controls. (B) Reciprocal bacterial two hybrid experiment (taken from the same plate) in which the T25 plasmids p25-N-*divIVA*, pKT25-*racA*, and p25-N-*minJ* were co-transformed into BTH101 along with pUT18 plasmids containing the DivIVA truncation series. This experiment confirmed the reduced interaction of DivIVAΔ26 and DivIVAΔ34 with full-length DivIVA. However, T25 fusions of RacA and MinJ did not reveal any interactions with DivIVA in this orientation.

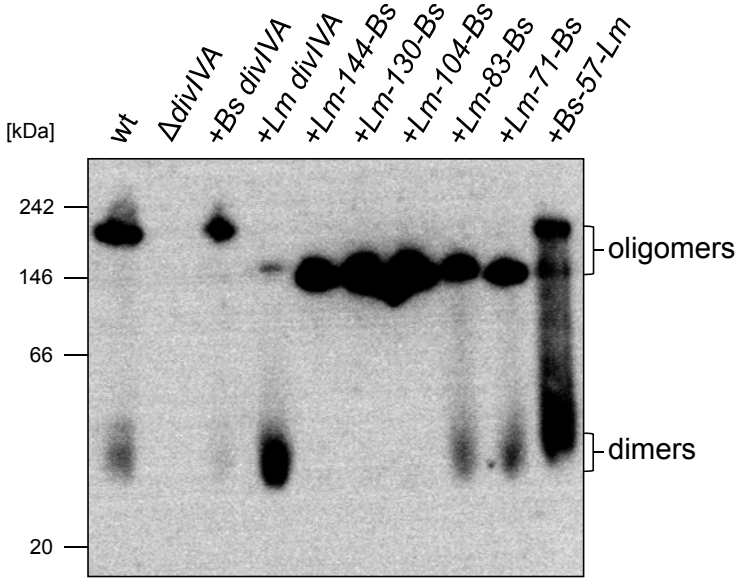

Fig. S2: Western blot after blue native PAGE to analyze oligomerization of chimeric DivIVA proteins. Strains expressing chimeric DivIVA proteins (BSN274: +*Lm*-144-*Bs divIVA*; BSN278: +*Lm*-130-*Bs divIVA*; BSN288: +*Lm*-104-*Bs divIVA*; BSN287: +*Lm*-83-*Bs divIVA*; BSN316: +*Lm*-71-*Bs divIVA*; BSN321: +*Bs*-57-*Lm divIVA*) were grown in LB broth supplemented with 0.5% xylose at 37°C and harvested in mid-logarithmic growth phase. Cell extracts were subjected to blue native PAGE, blotted onto a PVDF membrane and DivIVA proteins were immunostained using the anti-DivIVA antiserum. Strains 168 (wt), 4041 (Δ*divIVA*) and strains expressing the *B. subtilis* (BSN51) or the *L. monocytogenes divIVA* gene (BSN238) were used as controls. Please note that differences in the apparent molecular weight of the different DivIVA oligomers are explained by pI differences between *Bs* (pI 5.03) and *Lm* DivIVA (pI 4.77).During electrophoresis, which was performed at pH7.5, *Lm* DivIVA is more negatively charged as compared to *Bs* DivIVA and therefore runs faster through the gel even though its monomer has the higher theoretical molecular weight. Moreover, the pI values of the C-terminal domains of both proteins are nearly identical (*Bs* CTD: 4.93; *Lm* CTD: 4.80) whereas those of the N-terminal lipid binding domains are rather different (*Bs* LBD: 5.27; *Lm* LBD: 4.72). This explains why all chimeras containing the *Lm* LBD reveal the same apparent oligomer molecular weight as *Lm* DivIVA, whereas the *Bs*-57-*Lm* oligomer runs at the same position as *Bs* DivIVA.

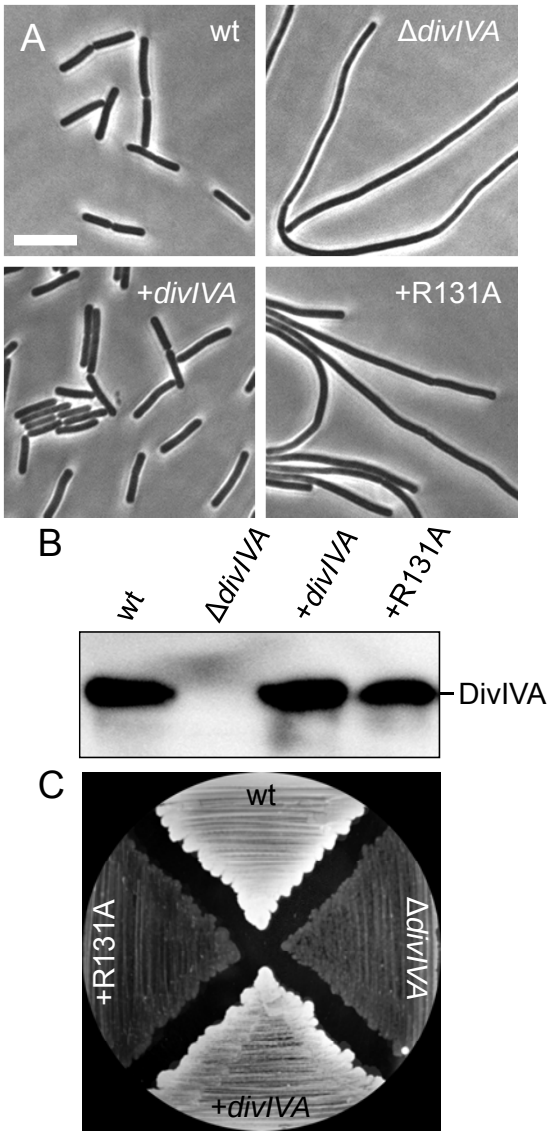

Fig. S3: A mutation in the tetramerisation domain (R131A) that causes an inactive *Bs* DivIVA protein. (A) Phase contrast micrographs obtained on cultures that were cultivated in LB broth containing 1 mM IPTG at 37°C during mid-logarithmic growth. Strains used were 168 (wt), 4041 (Δ*divIVA*), BSN5 (+*divIVA*) and BSN313 (+R131A). Scale bar is 5 µm. (B) Western blot on cell extracts of the same set of strains. DivIVA was visualised using the polyclonal rabbit anti-DivIVA antiserum. (C) The *divIVAR131A* mutant (strain BSN313) reveals a sporulation defect. Sporulation was assayed in a plate assay as described in the legend of Fig. 3B.

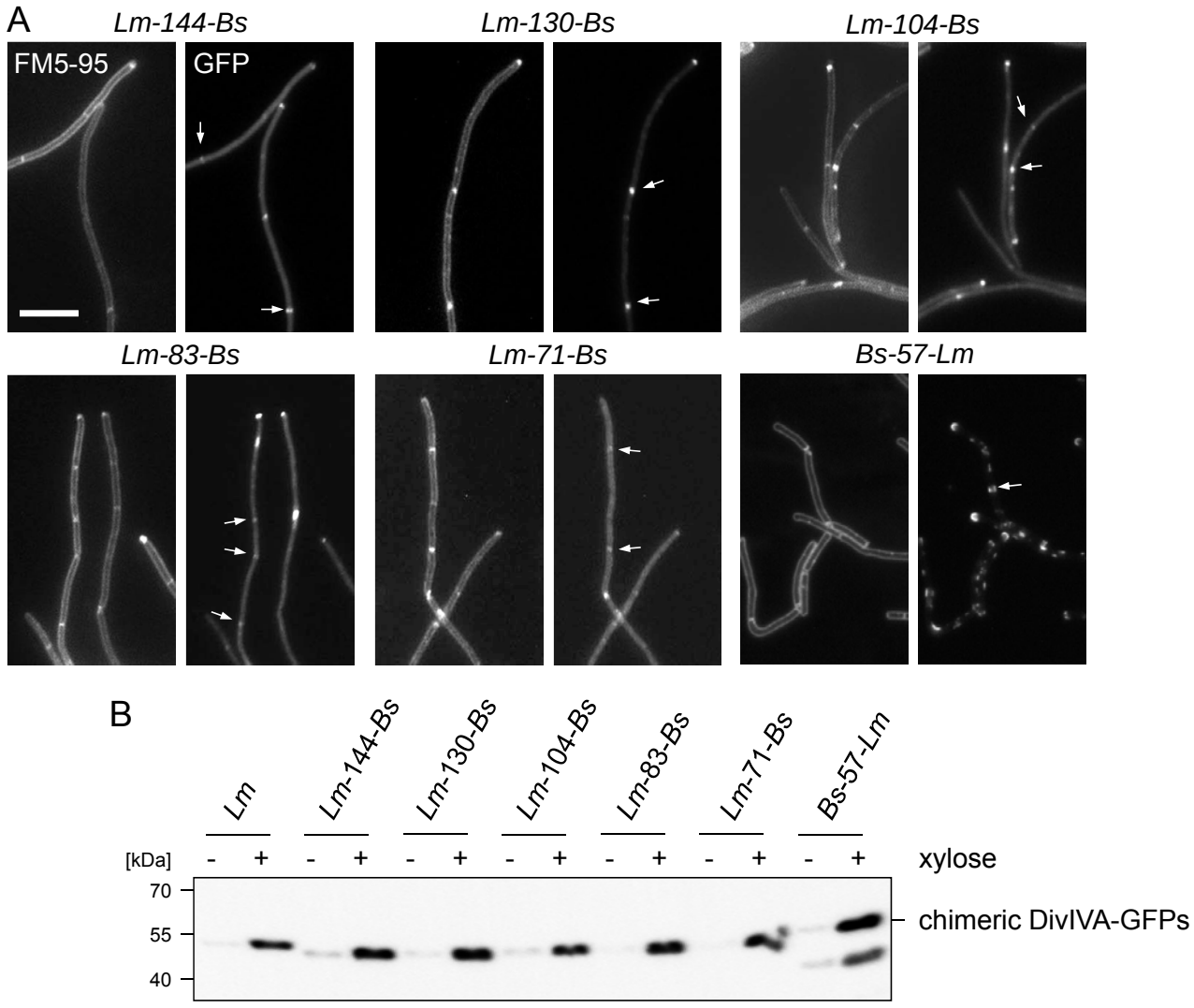

Fig. S4: Subcellular localisation of chimeric DivIVA proteins in a *B. subtilis* Δ*divIVA* background. Strains BSN294 (DivIVA$^{Lm\text{-}71\text{-}Bs}$-GFP), BSN295 (DivIVA$^{Lm\text{-}144\text{-}Bs}$-GFP), BSN296 (DivIVA$^{Lm\text{-}130\text{-}Bs}$-GFP), BSN297 (DivIVA$^{Lm\text{-}83\text{-}Bs}$-GFP), BSN298 (DivIVA$^{Lm\text{-}104\text{-}Bs}$-GFP), and strain BSN372 (DivIVA$^{Bs\text{-}57\text{-}Lm}$-GFP) were grown in LB supplemented with 0.5% xylose. DivIVA localisation patterns were analysed by epifluorescence microscopy (right images), and for orientation, FM5-95 stained images (left panels) were taken in parallel. Scale bar is 5 µm, septal DivIVA-GFP signals are indicated by arrows. All DivIVA-GFP fusions contain the *gfpA206K* mutation preventing GFP dimerization. (B) Western blot to demonstrate full-length expression of chimeric DivIVA-GFP proteins. Strains expressing chimeric DivIVA-GFP fusions were grown in LB broth containing or not containing 0.5% xylose to mid-logarithmic growth phase, total cellular proteins were isolated and subjected to SDS-PAGE and subsequent Western blotting. DivIVA-GFP fusion proteins were visualised using the polyclonal anti-GFP antiserum. Strains were as in panel A, but BSN373 (expressing *Lm* DivIVA-GFP) was also included. For convenience the names of the respective DivIVA chimeras are indicated above the blot. Please not that DivIVA$^{Bs\text{-}57\text{-}Lm}$-GFP shows some proteolytic degradation.

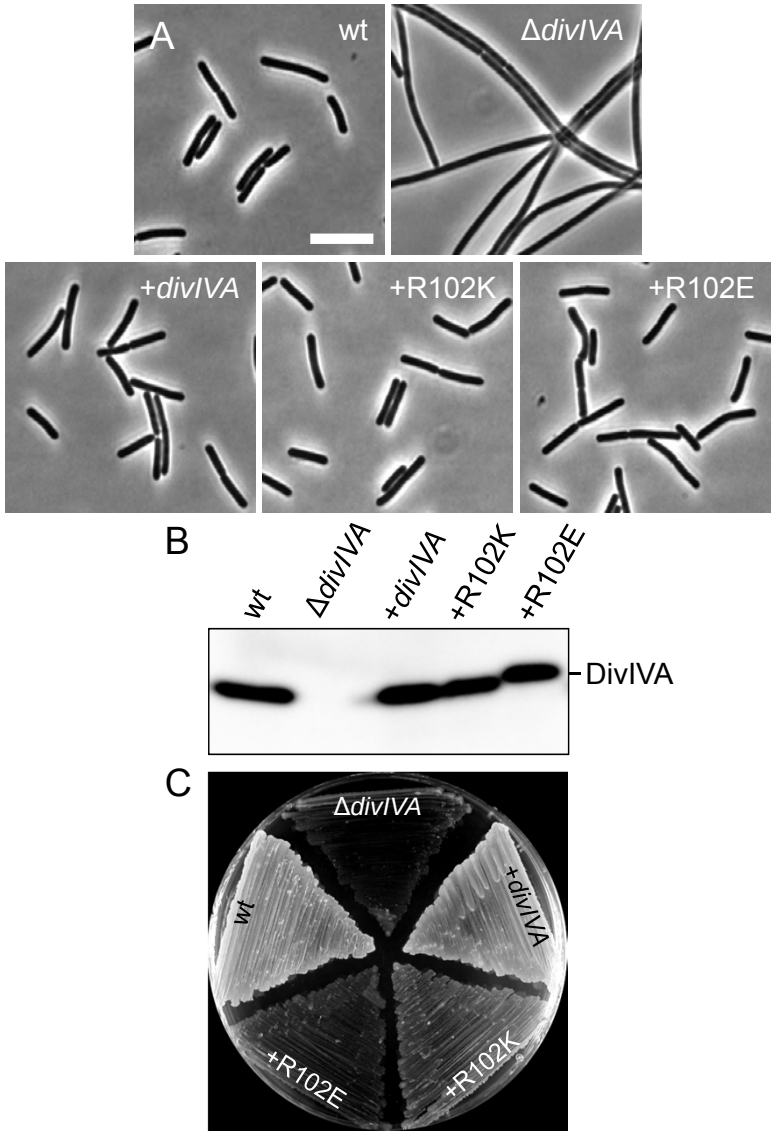

Fig. S5: Mutations of R102 in *Bs divIVA* cause a *div*$^{+}$ *spo*$^{-}$ phenotype. (A) Phase contrast micrographs obtained on cultures that were cultivated in LB broth containing 1 mM IPTG (where necessary) at 37°C during mid-logarithmic growth. Strains used for this experiment were 168 (wt), 4041 (Δ*divIVA*), BSN356 (+*divIVA*), BSN357 (+R102K), and BSN358 (+R102E). Scale bar is 5 µm. (B) Western blot on cell extracts of the same set of strains. DivIVA was visualised using the polyclonal rabbit anti-DivIVA antiserum. (C) Sporulation activity of the R102 mutants. Sporulation was assayed in a plate assay as described in the legend of Fig. 3. Please note that the sporulation defect of the phospho-ablative R102K mutant was less pronounced than that of the phospho-mimetic R102E allele.